LANGMUIR Article
Cite This: Langmuir XXXX, XXX, XXX−XXX
pubs.acs.org/Langmuir

Gas Hydrate Formation Probability Distributions: The Effect of Shear and Comparisons with Nucleation Theory

Eric F. May,*[,†] Vincent W. Lim,[†] Peter J. Metaxas,[†] Jianwei Du,[†] Paul L. Stanwix,[†] Darren Rowland,[†] Michael L. Johns,[†] Gert Haandrikman,[‡] Daniel Crosby,[§] and Zachary M. Aman[†]

[†]Fluid Science & Resources, School of Mechanical and Chemical Engineering, University of Western Australia, 35 Stirling Highway, Crawley, WA 6009, Australia

[‡]Shell Technology Centre Amsterdam, P.O. Box 3800, 1030 BN Amsterdam, The Netherlands

[§]Shell Technology Center Houston, P.O. Box 432, 3333 Highway 6 South, Houston, Texas 77210, United States

ABSTRACT: Gas hydrate formation is a stochastic phenomenon of considerable significance for any risk-based approach to flow assurance in the oil and gas industry. In principle, well-established results from nucleation theory offer the prospect of predictive models for hydrate formation probability in industrial production systems. In practice, however, heuristics are relied on when estimating formation risk for a given flowline subcooling or when quantifying kinetic hydrate inhibitor (KHI) performance. Here, we present statistically significant measurements of formation probability distributions for natural gas hydrate systems under shear, which are quantitatively compared with theoretical predictions. Distributions with over 100 points were generated using low-mass, Peltier-cooled pressure cells, cycled in temperature between 40 and −5 °C at up to 2 K·min^{-1} and analyzed with robust algorithms that automatically identify hydrate formation and initial growth rates from dynamic pressure data. The application of shear had a significant influence on the measured distributions: at 700 rpm mass-transfer limitations were minimal, as demonstrated by the kinetic growth rates observed. The formation probability distributions measured at this shear rate had mean subcoolings consistent with theoretical predictions and steel−hydrate−water contact angles of 14−26°. However, the experimental distributions were substantially wider than predicted, suggesting that phenomena acting on macroscopic length scales are responsible for much of the observed stochastic formation. Performance tests of a KHI provided new insights into how such chemicals can reduce the risk of hydrate blockage in flowlines. Our data demonstrate that the KHI not only reduces the probability of formation (by both shifting and sharpening the distribution) but also reduces hydrate growth rates by a factor of 2.

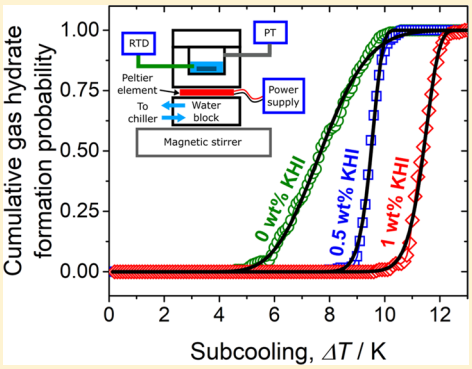

INTRODUCTION

As the use of subsea oil and gas flowlines moves toward increasingly deeper water, the risk of gas hydrate formation during both steady-state and transient operations grows accordingly.[1] Although much effort has been expended in the last four decades to improve hydrate phase boundary predictions for a wide range of gas and aqueous phase compositions, only limited data are available to describe the stochastic nature of hydrate formation once a system enters the hydrate stability region.[2−4] The probability of hydrate formation increases with both the subcooling below the equilibrium temperature and the (induction) time spent inside the hydrate stability region. However, most engineering tools available for assessing the blockage risk in production systems rely on highly simplified heuristics for estimating whether hydrates will form or not. For example, the flow assurance software tool, OLGA-CSMHyk,[5] uses a widely accepted industry heuristic based on the average of five field tests conducted on the Werner Bolley well,[6] which simply assumes that hydrates will nucleate when the subcooling exceeds 3.6 K (6.5 °F). Although such an approach may be useful as a first approximation, the use of a single subcooling value without reference to induction time clearly precludes precise quantification of hydrate formation risk in system design.

Operational flow assurance strategies based on low-dose kinetic hydrate inhibitors (KHIs) are increasingly being deployed.[7−10] These strategies rely on delaying hydrate formation beyond both a subcooling threshold (e.g., 10 K) and a minimum induction time (e.g., 120 h).[11] Although experiments with rocking cells and autoclaves can be used to conduct performance tests and rank potential KHI chemicals and concentrations,[12] the application of results obtained in such laboratory experiments to operations in the field currently relies on company- and/or vendor-specific heuristics. As a consequence, this limits the generality and extent to which KHI-based operating strategies can be assessed and systematically applied.

Advancing this state of affairs requires an improvement in the ability to describe fundamentally hydrate formation probability. Nucleation theory[13] offers the framework necessary for such a

Received: November 13, 2017
Revised: February 5, 2018

DOI: 10.1021/acs.langmuir.7b03901
Langmuir XXXX, XXX, XXX−XXX

general quantitative description and, potentially, could be used to predict hydrate formation probability as a function of induction time, subcooling, and KHI concentration within a flowline. Starting in 2002, Kashchiev and Firoozabadi published three seminal papers[14−16] in which nucleation theory was used to provide quantitative expressions for the driving force, nucleation rate, and induction time of methane hydrates under various scenarios, including the influence of KHI concentration. However, despite the extensive framework presented, there have been few applications of the theoretical models presented by Kashchiev and Firoozabadi in the subsequent 15 years.[17−19]

One possible reason for the limited use of these models may be the difficulty of producing experimental hydrate formation data with uncertainties small enough to allow for meaningful comparisons with theory. A particular challenge is the generation of statistically significant numbers of hydrate formation events within a practical time frame. This challenge is linked with the need to cycle pressure vessels over a temperature range of around 10−30 K, as the system under study is moved from outside the hydrate stability region to a target subcooling condition and then back. Typical cooling rates for the most commonly used apparatus for studying hydrate formation and qualifying KHIs, namely, high-pressure (HP) rocking cells and stirred autoclaves,[4,20] are limited to between 1 and 6 $K{\cdot}h^{-1}$. Consequently, the time frame for a single formation cycle generally is on the order of hours. As a result, formation distributions reported in the literature typically consist of only 10−40 points. The fractional statistical uncertainties arising solely from distributions with this number of points will be in the range of 30−15%.

To address this issue, Haymet, Wilson, and co-workers[21,22] developed the automated lag time apparatus (ALTA) to study ice and hydrate nucleation at ambient pressure, which was capable of cooling at rates up to 4.5 $K{\cdot}min^{-1}$, thereby enabling the acquisition of large numbers of formation events in a practical time frame (≈100 in 30 h). Subsequently, Maeda and co-workers[3,23,24] developed a high-pressure (HP-)ALTA to study the kinetics of hydrate formation from methane + propane gas mixtures. May et al.[25] used this HP-ALTA to study the memory effect and rank the performance of six KHIs; the results of the inhibitor testing with the HP-ALTA matched the ranking determined using rocking cells but with additional insights derived from the more detailed formation probability distributions. However, the samples under study in the HP-ALTA were quiescent and, consequently, large subcoolings of 10−30 K were observed, with the distributions that were obtained being particularly susceptible to inadvertent influence by the memory effect. Moreover, the detection of hydrate formation was based on monitoring changes in the optical transmissivity of the sample. Such an approach makes estimating the minimum detectable amount of hydrate difficult, limits the ability to conduct studies of growth, and prevents any ability to discriminate between ice and hydrate formation, which is particularly important at high subcoolings. Maeda and co-workers[26,27] also developed a version of the HP-ALTA in which hydrate formation was inferred from changes in the electrical conductivity of a saline aqueous phase; however, this approach does not really address the above limitations, which are caused by the difficulty of quantitatively linking the detection method to the type or amount of solid phase formed.

Here, we report the development of a high pressure, stirred, and automated lag time apparatus, (HPS-ALTA), which overcomes both of these key limitations. It combines the advantages of autoclaves and rocking cells, namely, the ability to apply shear and use of a pressure-based detection system, with the rapidity of temperature cycling that enables the automated measurement of formation probability distributions with statistical significance in practical time frames. This HPS-ALTA, when combined with an automated data-processing algorithm, enables the probability of gas hydrate formation to be efficiently determined as a function of key operational parameters, such as system temperature, subcooling, shear rate, gas composition, and liquid composition, with the latter including inhibitors at various concentrations. In addition, the measured hydrate formation probability distributions are analyzed using the theoretical framework of Kashchiev and Firoozabadi[14,16] as a first step toward generalizing what may conventionally be considered as apparatus-specific data into results of more fundamental significance and/or industrial relevance.

EXPERIMENTAL SECTION

Apparatus and Method. A schematic and photo of the HPS-ALTA is shown in Figure 1. Each of the two cells within the system consists of a machined, cylindrical, stainless steel well of volume 4.63 mL, diameter 20.1 mm, and depth 14.6 mm, sealed with a nitrile O-ring (Ludowici Sealing Solutions) by an upper plate containing a sapphire window (WG31050, Thorlabs, Inc.; visible in Figure 1b). A polytetrafluoroethylene−glass fiber (PTFE−GF) O-ring is used to make a seal between the upper surface of the sapphire window and the steel lid. Magnetic

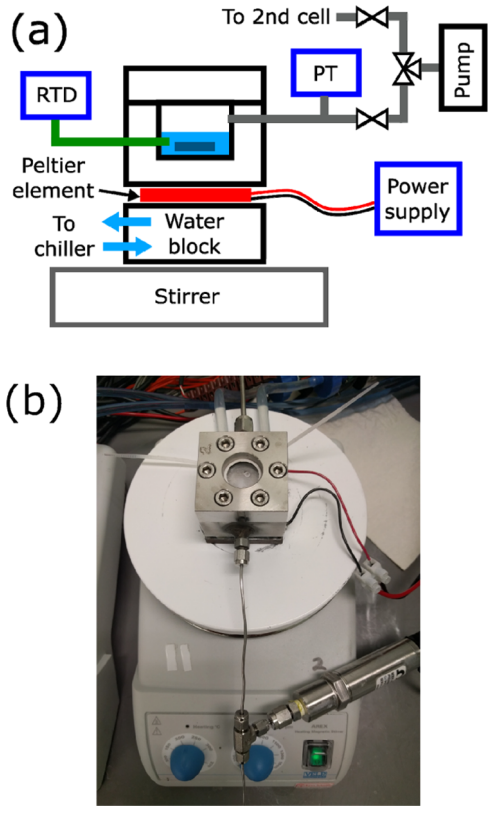

Figure 1. HPS-ALTA system. (a) System schematic (RTD: resistance temperature detector, PT: pressure transducer). The gray rectangle within the cell represents the stirring bar. The RTD, PT, and Peltier power supply (marked in blue) are interfaced with a computer for temperature control and data acquisition. (b) Top-down view of one of the HPS-ALTA cells. The stirrer, PT, part of the RTD (top of the image), and the wires that provide power to the Peltier element are also visible.

DOI: 10.1021/acs.langmuir.7b03901
Langmuir XXXX, XXX, XXX−XXX

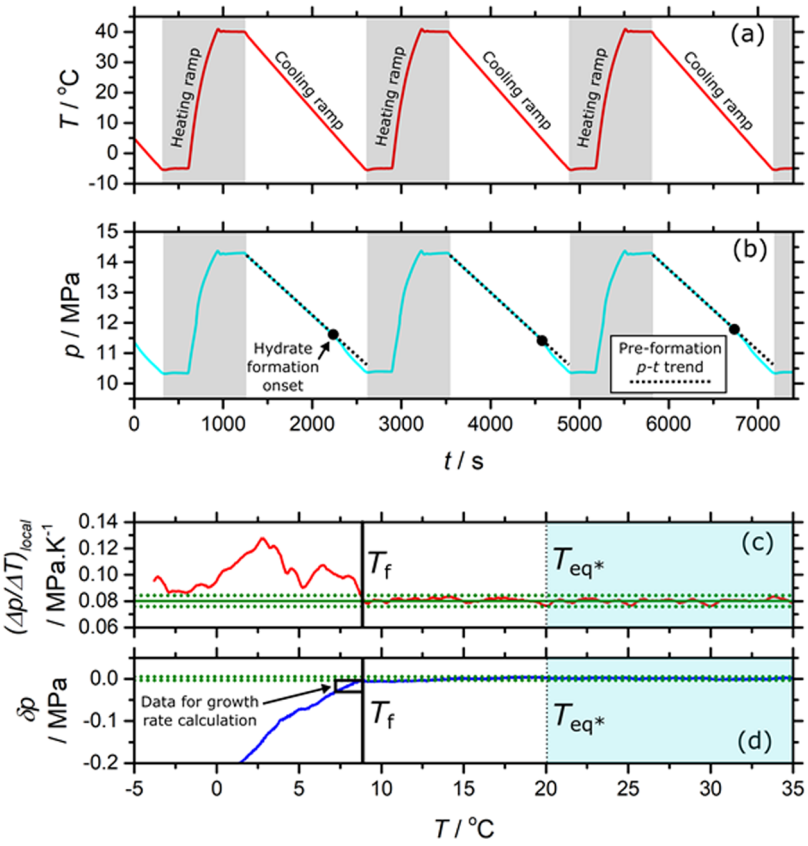

Figure 2. (a) Temperature and (b) pressure−time series data from the HPS-ALTA for three complete hydrate formation−dissociation cycles (gas mixture, 100 rpm, 2 K·min^{-1} cooling rate; initial conditions: 13 MPa at 20 °C). Hydrate formation can be identified in (b) from the resulting increased pressure drop, which occurs toward the end of the cooling ramp. (c, d) Result of automated analysis of the (p, T) time series data obtained during a single cooling ramp for the gas mixture. The red line in (c) shows the calculated $(\Delta p/\Delta T)_{local}$ values, whereas the blue line in (d) corresponds to the $\delta p = p - p_{isochor}$ values. The solid green line (which for clarity is only shown in (c)) corresponds to the mean value of that quantity above T_{eq^*}, whereas the dashed green lines show the (mean $\pm 3\sigma$) boundaries. In this data set, T_f was determined using the $(\Delta p/\Delta T)_{local}$ data, yielding a value of 8.7 °C, which matches well with the onset of unambiguous gas consumption that can be seen in (d). The blue shaded regions in (c, d) correspond to those temperatures for which the system was outside of the hydrate equilibrium region of the $p-T$ phase space. The δp data within the black outlined box were used to calculate the initial gas consumption rate due to hydrate formation (0.6 kPa·s^{-1}).

stirrers (AREX, Velp Scientifica Srl) drive a PTFE-coated, cylindrical magnetic stirring bar (13 mm long, 6 mm wide; Cowie Technology Group Ltd.) within each cell at a specified rate, enabling shear to be applied continuously to the fluid during the experiment. The actual rotational speed achieved for a given setting between 100 and 700 rpm was confirmed with a laser-based tachometer (DT-2236B, Lutron Electronic Enterprise Co., Ltd.). The energy delivered to the aqueous phase as a result of viscous dissipation by the stirrer at 700 rpm was estimated to be less than 66 mW, which is negligible in comparison with the cooling power applied to the cell by the Peltier element (10−20 W).

In each cell, a Peltier element was situated between the cell's outer bottom surface and a coolant block through which chilled ethylene glycol or water was circulated via a LAUDA Alpha RA8 cooling thermostat. The Peltier elements (ET-161-12-14-E, Adaptive Thermal Management) were driven by programmable power supplies (E3648A, Agilent Technologies), enabling independent control of each cell's temperature. To achieve this control, the temperature of the liquid within each cell was measured using a Pt-100 resistance temperature detector (RTD) (Omega Engineering Limited, uncertainty: 0.1 K). The RTD reading was used in a digital feedback loop to set the output voltage of the Peltier power supplies. The gas phase pressure within each cell was also continuously monitored using a pressure transducer with a full-scale of 23.5 MPa (MM Series, Omega Engineering Limited; relative uncertainty: 0.08% of full-scale). Both pressure and temperature transducer signals were monitored using a National Instruments data acquisition system connected to a computer running the LabVIEW software package.[28]

Measurements were conducted by first loading each of the open cells with 1 mL of deionized water. The cells were then sealed and pressurized using a syringe pump (Teledyne Isco) to a specified initial pressure at 20 °C with either methane (99.995% purity) at 8.5 MPa or a gas mixture ($0.9036CH_4 + 0.0571C_2H_6 + 0.019C_3H_8 + 0.02CO_2$, where the fractions are on a molar basis) at 13 or 8.5 MPa. Unlike in the atmospheric pressure ALTA studies by Wilson et al.[21] no catalysts were used to promote nucleation. Following pressurization, the cells were then isolated from each other, enabling the simultaneous collection of two independent data sets. The cell contents were stirred continuously at the specified shear rate throughout the experiment. Initially, the cell was heated to a specified regeneration temperature, T_{regen}, where it was maintained for a period of 5 min, which was more than sufficient for the pressure to stabilize. The cells were then cooled at a fixed rate before being held at the target minimum temperature (typically −5 °C) for 5 min. Finally, the cell was heated at a rate of 8.5 K·min^{-1} back to T_{regen}, where it was maintained for a specified hold time, t_{hold}, (typically 5 min) before the cooling ramp was repeated. Between each ramp, the pressure at which the cell stabilized during t_{hold} at T_{regen} allowed confirmation that no leaks had developed over the course of the experiment's duration. These cooling/heating cycles were repeated continuously for a period of between 24 and 48 h until a statistically significant number of hydrate formation events had occurred (typically on the order of 100).

Formation and Growth-Rate Probability Distributions. Hydrate formation was detected via analysis of the temperature and pressure−time series data recorded for each cooling ramp. Figure 2 shows an example of these temperature and pressure data, as obtained

DOI: 10.1021/acs.langmuir.7b03901
Langmuir XXXX, XXX, XXX−XXX

for the gas mixture under a 100 rpm shear for a cooling rate of 2 K·min^{-1}. Three full hydrate formation−dissociation cycles are shown, with each temperature−time series clearly separated into the stages described above (heating and cooling ramps separated by nearly isothermal waiting periods). Hydrate formation events during the cooling ramp can be identified in Figure 2b from changes in the slope of the pressure−time series data.

To construct a formation probability distribution, the temperature at which the formation event occurred was identified for every one of the 100 or so cycles that comprised a single experiment. A hydrate formation detection algorithm was developed to minimize subjectivity and reduce analysis time and implemented using the Python language with the pandas,[29] matplotlib,[30] and numpy[31] packages. An example of the analysis conducted using the automated detection algorithm is shown in Figure 2c,d. As a first step, the measured pressure was used to assess whether the system was inside the hydrate stability region by calculating the corresponding equilibrium temperature, T_{eq}, using the Cubic Plus Association (CPA) model implemented in the software package Multiflash 4.4 and comparing it with the measured temperature at that point on the cooling ramp (the CPA model predictions of the gas mixture's hydrate equilibrium temperature were verified within 0.2 K in separate experiments using a sapphire autoclave in our laboratory, following the method detailed by Akhfash et al.[32]). The isochoric measurement pathway meant that once the system had been cooled to a temperature equal to the value of T_{eq} calculated from the measured pressure, the system would be within the hydrate stability region at any lower temperature. This condition, identified as T_{eq^*}, was common to all cooling ramps measured with the same overall density (i.e., for cells with no leaks). The pressure−temperature data measured for the cooling ramp outside the hydrate stability zone were used to determine a baseline slope, $(\Delta p/\Delta T)_{isochor}$, characteristic of the isochoric cooling of the system. Hydrate formation was then determined by identifying the condition at which the (p, T) series data measured within the equilibrium region (i.e., $T < T_{eq^*}$) exhibited a statistically significant deviation (99.7% confidence interval or 3 standard deviations) from the trend extrapolated using $(\Delta p/\Delta T)_{isochor}$.

Two methods were used to detect local deviations of the (p, T) series data from the baseline trend extrapolated using $(\Delta p/\Delta T)_{isochor}$. The first method used a numerical calculation of the local slope, $(\Delta p/\Delta T)_{local}$, at every 0.05 K along the cooling ramp via linear regression of the (p, T) series data within a 0.5 K window (Figure 2c). The second method calculated the deviation in pressure, $\delta p = p - p_{isochor}$, of each measured ($p$, T) data point from the linearly extrapolated pressure $p_{isochor}$ at the same temperature estimated using $(\Delta p/\Delta T)_{isochor}$ and the data measured above T_{eq^*} (Figure 2d). Standard deviations for both of these quantities, $\sigma_{\Delta p \Delta T}$ and $\sigma_{\delta p}$, were calculated from the data acquired on the section of the cooling ramp measured outside the hydrate stability region. In both methods, the formation condition was identified as being the first point on the cooling ramp, where 20 consecutive values of that quantity ($(\Delta p/\Delta T)_{local}$ or δp) differed by more than 3 standard deviations from the baseline trend extrapolated using $(\Delta p/\Delta T)_{isochor}$. In general, the first method tends to produce a leading estimate of the formation temperature, T_f, (i.e., one which is too high) because of the finite-width fitting window used to evaluate $(\Delta p/\Delta T)_{local}$ (the calculated local slope at a given temperature is influenced by data obtained at slightly lower temperatures). In contrast, the second method tends to produce a lagging estimate of the formation temperature (i.e., one which is too low) because of the requirement for δp to become larger than $3\sigma_{\delta p}$. Detection via the second method can also be less reliable as a result of the cumulative drift in δp resulting from small but consistent incremental deviations, which cause the signal to move slightly outside the extrapolated baseline trend, resulting in an erroneous identification of hydrate formation. Each data set was analyzed using both methods; in general, we found method 1 to be more reliable in comparison with a manual assessment of the same data set to identify the formation point (as is the case for the data shown in Figure 2). Accordingly, we used the first method but reviewed manually all instances where a discrepancy of more than 0.2 K existed between the formation points determined by each method. In those cases, the manual review usually identified one or other method as giving a better identification of the formation point, although in some instances an arithmetic average of the values determined via each of the methods was used. To facilitate this inspection, the code was written to enable live visualization of the $p-T$ data around the extracted formation temperature for each cooling ramp during the automated analysis.

On occasion, the formation of hydrates was also indicated by a spike in the reading of the temperature sensor in contact with the water at the same time or shortly after they were detected from the pressure signal. However, this did not prove to be a reliable indicator because the response of the thermometer was dominated by the smoothly ramped temperature of the cell wall (a further indication of efficient stirring). Additionally, the magnitude of any temperature rise depended on the proximity of the sensor to the location of the hydrate formation.

For each formation event, the subcooling temperature, ΔT, was calculated by subtracting the formation temperature away from the calculated equilibrium temperature at the formation pressure, i.e., $\Delta T = T_e - T_f$. Subcooling probability distributions were then constructed using the method detailed by May et al.,[25] by first constructing a histogram with a bin width of 0.1 K (equal to the temperature sensor uncertainty). An upper limit for the subcooling achieved across all experiments was chosen, so that the histograms constructed for different experiments could be represented as arrays of the same length, with the same spacing. This allows subsequent numerical operations on the histograms, such as integration or subtraction, to be performed in a straightforward manner. Cumulative formation probability distributions were then constructed by numerically integrating the histograms via the trapezoidal rule.

The use of the pressure signal enables hydrate formation to be distinguished from ice formation. Despite its exothermic nature, hydrate formation results in a pressure decrease due to gas consumption, whereas ice formation results in a small increase in gas phase pressure due to the slightly lower density of ice relative to that of water and the heating of the gas phase. Distinguishing these two phases can be problematic at temperatures below 0 °C for those experimental techniques that rely, for example, upon optical detection of the hydrate phase.[25]

The minimum detectable amount of hydrate can be estimated from the noise floor of the pressure transducer, which was 0.001 MPa at a constant temperature and 8 MPa with a data acquisition rate of 1 Hz (the response time of the pressure transducer was much shorter than the data acquisition rate). During a cooling ramp, the standard deviation, $\sigma_{\delta p}$, was usually slightly larger than this noise floor at about 0.002 MPa (e.g., as in Figure 2d). Given that the volume of the gas phase in the system was approximately 3.5 mL (accounting for the volume of the water, stirrer, and gas-containing tubing), the minimum detectable amount of gas consumption corresponding to $3\sigma_{\delta p}$ (0.005 MPa) was about 9 μmol at 283 K. Assuming eight guest molecules per unit cell of sI hydrates,[2,33] this corresponds to a minimum detectable amount of hydrate of 1.1 μmol, which for CH_4 hydrate would have a mass of 19.5 μg. If this small amount of hydrate formed at the kinetic rate calculated using the correlation of Turner et al., on the basis of the measurements of Vysniauskas and Bishnoi and Englezos et al.,[5,34,35] the time lag required for detection would be 2.9 s.

Another advantage of the present technique is that the recorded pressure−time series data can be used to determine the rate of gas consumption immediately following the detected formation event, thus enabling a quantification of the initial hydrate growth rate, G (e.g., as in ref 34). This information is useful, for example, when assessing the ability of KHIs to suppress hydrate growth separately to their ability to delay hydrate formation.[12] Such data allow the measured growth rate to become an important, additional performance metric for KHIs, which can be more difficult to quantify with other testing methods. Although any apparatus with a pressure gauge, such as rocking cells or an HP-ALTA using optical detection, can in principle determine a rate of gas consumption, accurately determining the initial growth rate requires a precise determination of gas consumption immediately after the start of hydrate formation. The HPS-ALTA described in this work identifies the moment of formation within 3 s, whereas optical HP-ALTA systems reported to date typically require up to 1 min. In contrast, before a formation event can be determined in a rocking cell, an unknown and

DOI: 10.1021/acs.langmuir.7b03901
Langmuir XXXX, XXX, XXX−XXX

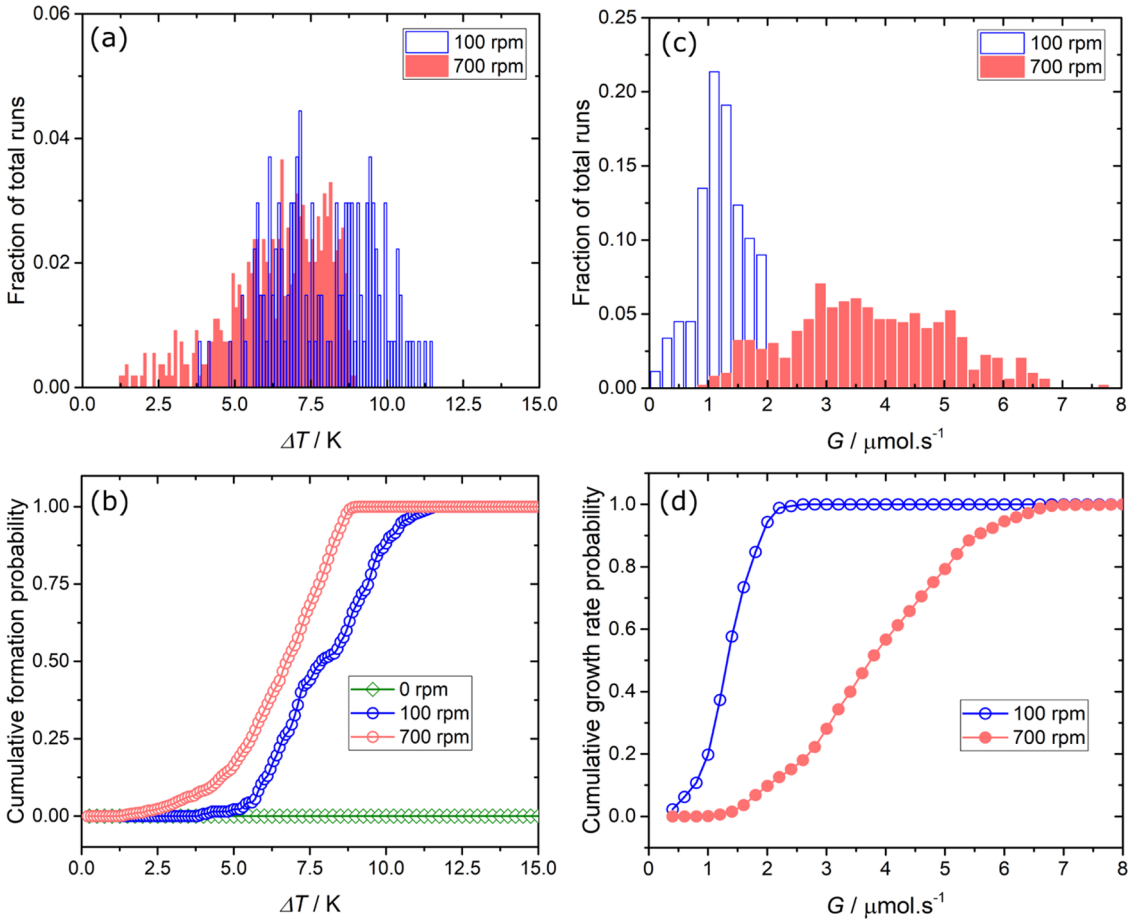

Figure 3. Hydrate formation and growth-rate probability distributions for CH_4 under varying levels of shear for an initial condition of 8.5 MPa at 20 °C and a regeneration temperature of 40 °C. (a) Probability density of hydrate formation and (b) calculated cumulative formation probability versus subcooling, ΔT. Note that no hydrate formation was observed during the quiescent (0 rpm) experiment even at subcoolings of 15 K. The distributions were constructed from 135 measurements at 100 rpm and 547 measurements at 700 rpm. (c) Probability densities and (d) calculated cumulative probability functions for initial hydrate growth rates, G, (as quantified by the rate of gas consumption).

variable amount of hydrate must form to prevent the ball within the rocking cell from moving. Moreover, this initial growth rate can be determined with the HPS-ALTA following each event used to construct the formation probability distribution, making construction of a growth-rate distribution from the same data set relatively simple.

To determine the initial growth rate immediately following each formation point, the δp values calculated as part of method 2 above were used to assess the rate at which the decrease in pressure exceeded the baseline trend of the isochore. The initial gas consumption rate was extracted from a linear fit to a subset of the $\delta p - T$ data, shown as a boxed area in Figure 2d, starting at the formation point and stopping once the δp decreased by a specified threshold amount, which in this work was chosen to be 30 kPa. The magnitude of this threshold must be chosen to be significantly larger than the noise floor in the δp data but also sufficiently small such that (i) it is reached in all cooling ramps and (ii) the observed growth rate is not slowed by the onset of heat and mass-transfer limitations. Growth-rate probability distributions were then constructed with a method similar to that used for the formation probability distributions: a histogram with a bin width of 0.2 μmol·s^{-1} was constructed for the gas consumption rate, and a maximum gas consumption rate applicable across all experiments was chosen to ensure uniformly spaced cumulative probability distributions were produced by numerical integration of the histograms.

RESULTS AND DISCUSSION

Impact of the Shear Rate. The apparent driving force required for hydrate formation could be expected to increase with decreasing levels of shear, as mass-transfer limitations restrict the rate of gas supersaturation in the aqueous phase. Indeed, the formation probability distributions measured by Maeda and co-workers[25] using quiescent HP-ALTA experiments with a methane + propane mixture had median subcoolings around 14 K, increasing to 27 K when kinetic hydrate inhibitors were added to the aqueous phase. Ke and Svartaas[19] examined the impact of shear using an autoclave and observed that increased shear rates shifted the average subcooling down; however, the number of data points in those distributions was limited to 10 due to the low achievable cooling rate. Consequently, the three data sets acquired by Ke and Svartaas[19] did not exhibit a clear trend, with the average subcooling measured at 440 rpm being smaller than the averages at both 220 and 660 rpm.

The HPS-ALTA was used to measure formation probability distributions for the CH_4–water system at three shear rates: 0, 100, and 700 rpm. The resulting formation histograms and cumulative probability distributions are shown in Figure 3. No unambiguous formation events were detected for the quiescent experiment, even at subcoolings as large as 15 K, which represented the limit of the measurement range for methane (around −5 °C). However, with the application of some shear, statistically robust formation probability distributions could be acquired: at 100 rpm, 135 data points were acquired with an

DOI: 10.1021/acs.langmuir.7b03901
Langmuir XXXX, XXX, XXX−XXX

average subcooling of 7.94 ± 0.14 K, where the error bound denotes the statistical uncertainty of the mean (i.e., $\sigma/\sqrt{N}$, where σ is the standard deviation of a distribution with N points). At 700 rpm, 547 data points were acquired with an average subcooling of 6.44 ± 0.07 K. Although application of the maximum achievable shear rate (700 rpm) led to the lowest mean subcooling observed in our experiments, the shift caused by increasing the shear rate from 100 to 700 rpm was at least 7 times smaller than the shift caused by increasing the shear rate from 0 to 100 rpm. This substantial reduction in the shift of the subcooling distribution caused by further increases in shear implies that formation probability measurements made with the HPS-ALTA at 700 rpm are approaching those for systems without mass-transfer limitations. Thus, our results indicate that the application of even a small amount of shear within the HPS-ALTA cell can strongly reduce the mass-transfer limitations that afflict quiescent experiments.

Figure 3c,d shows the cumulative probability distributions measured for CH_4 hydrates and the corresponding histograms for initial growth rates at 100 and 700 rpm, respectively. The measured distributions further demonstrate how the application of shear reduces mass-transfer limitations on hydrate growth, with the average of 1.22 ± 0.04 μmol·s^{-1} observed at 100 rpm, increasing to an average of 3.71 ± 0.06 μmol·s^{-1} at 700 rpm. The initial growth rate at 100 rpm was lower than that at 700 rpm despite the growth occurring at a higher average subcooling; this implies the growth rates observed at 100 rpm were limited by mass-transfer limitations. In contrast, the average growth rate measured at 700 rpm is in excellent agreement with the kinetic rate of 3.0 μmol·s^{-1} predicted at the average subcooling using the correlation of Turner et al.[5] if the available surface area for growth is taken to be 6 cm^2 on the basis of the wetted area of the cylindrical cell. Estimating the interfacial area involved in such reactions is always difficult: the steel−water interface was used in this calculation because (i) it is the interface where nucleation is predicted to be most likely[14] and (ii) use of the 3.2 cm^2 gas−water interfacial area leads to a kinetic growth-rate prediction of only 1.6 μmol·s^{-1}, which is far less than that observed. Regardless of which interfacial area is chosen, the growth rates observed provide further evidence that hydrate formation measurements made with the HPS-ALTA at shear rates of 700 rpm approached those corresponding to systems without mass-transfer limitations.

Although probability distributions containing 100−200 hydrate formation events have been measured previously using ALTA cells,[3,24,25] the repeatability of those measured distributions has generally not been considered. In this work, we attempted to establish the repeatability of measured formation and growth-rate probability distributions, each containing a similar, statistically significant number of data. Figure 4 shows the results of five separate experiments where formation and growth-rate probability distributions each containing 67−204 data points were measured independently over a 6 month period. Also shown are the cumulative probability distributions produced by combining each of the five independent data sets; these are the same as the 547 point distributions measured for CH_4 at 700 rpm shown in Figure 3. The individual formation probability distributions have averages ranging from 5.6 ± 0.2 to 7.1 ± 0.2 K, with standard deviations ranging from 1.3 to 1.9 K. The growth distributions have mean values in the range 3.2 ± 0.1 to 4.3 ± 0.2 μmol·s^{-1}, with standard deviations that range from 1.1 to 1.4 μmol·s^{-1}.

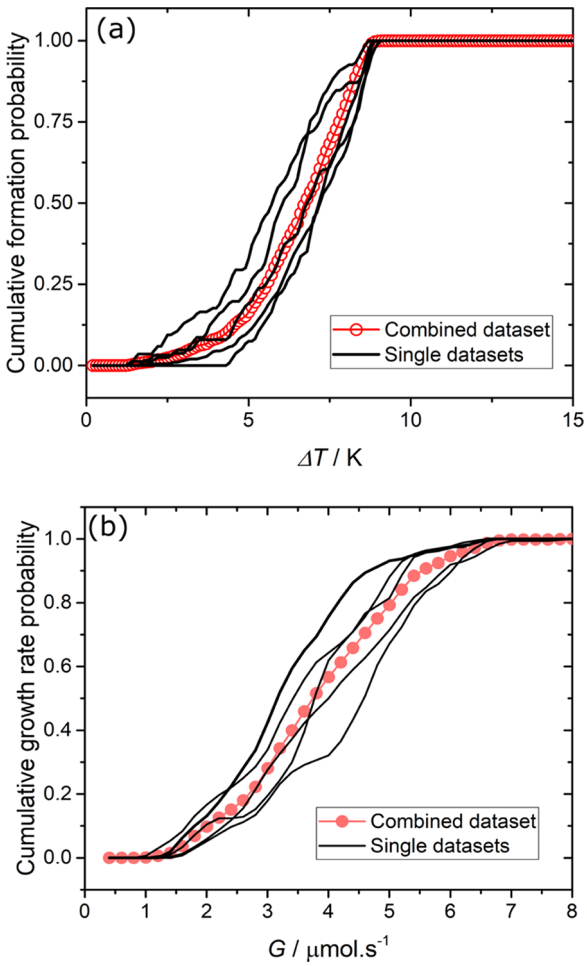

Figure 4. Repeatability of CH_4 hydrate probability distributions measured with the HPS-ALTA for (a) formation (plotted versus subcooling, ΔT) and (b) growth rate, G, as quantified by the rate of gas consumption. The variation of five separate measurements of distributions each containing 67−204 points acquired over a 6 month period is shown, together with the cumulative distribution produced by combining the separate data sets. Data shown are for an initial condition of 8.5 MPa at 20 °C and a regeneration temperature of 40 °C.

Although the results shown in Figure 4 indicate the level of reproducibility that can be expected for the current HPS-ALTA experiments when maximum shear is applied, they also show that the repeatability of the measured distribution averages is worse than that which might be expected from purely statistical estimates of its uncertainty. Fluctuations in the mean (derived from about 100 formation measurements) were typically about the same as or slightly smaller than the standard deviation of the underlying distribution (i.e., 1−2 K). Experiments conducted with two different HPS-ALTA cells in the same laboratory over several months were observed to produce distributions consistent at the level of 3 K or better if their surface finish, volume, geometry, stirring mechanisms, shear rate, water quality, and environmental conditions were similar. Variations in any of these factors were found to produce shifts in the distributions significantly larger than those exhibited in Figure 4.

Nucleation Theory for Comparisons with Experiment. Kashchiev and Firoozabadi[14] analyzed hydrate nucleation in binary gas + water systems and presented several key theoretical results. These included expressions for the driving force for nucleation in terms of the supersaturation, $\Delta\mu$, of gas−water

DOI: 10.1021/acs.langmuir.7b03901
Langmuir XXXX, XXX, XXX−XXX

solutions along isobaric and isothermal pathways in terms of system over-pressure and subcooling, respectively, as well as the work required to form a cluster of n hydrate "building units" in either the bulk of the aqueous phase (homogeneous nucleation), at the water−gas interface, or at the interface between the water and solid substrate containing it (heterogeneous nucleation). These expressions indicate that heterogeneous nucleation, as might be expected to occur on the stainless steel cell walls, is more energetically favorable than nucleation either in the bulk solution or on the water−gas interface. This result depends, however, quite sensitively on the hydrate−substrate surface energy which influences both the size and shape of the cluster,[13] an effect which is taken into account below via the factor, Ψ, which in turn depends on the contact angle, θ, between the substrate, the hydrate, and the fluid phase.

By comparing the work required for the formation of a critically sized cluster with the available, driving force, $\Delta\mu \approx \Delta s_e\, \Delta T$, where Δs_e is the entropy of hydrate dissociation at T_e, Kashchiev and Firoozabadi derived expressions for the rate at which critically sized nuclei will appear. At constant pressure, the nucleation rate, J, is said to be stationary or time-independent if the subcooling (and hence temperature) is constant, and may be calculated using

$$J(\Delta T,\, T) = A\, \exp\left(\frac{\Delta s_e\, \Delta T}{k_B T}\right) \exp\left(-\frac{B'}{T\Delta T^2}\right) \tag{1}$$

Here, A and B' are referred to as the kinetic and thermodynamic parameters, respectively. The kinetic parameter is so named because it accounts for the attachment mechanism of the hydrate building units to the nucleus and, to a first approximation, can be taken to be independent of subcooling. The kinetic parameter A has the same dimensions as those of the nucleation rate (e.g., $m^{-3}\cdot s^{-1}$ for homogeneous nucleation in a bulk solution or $m^{-3}\cdot s^{-1}$ for heterogeneous nucleation on a substrate) and is given by the general form

$$A = zfC_0 \tag{2}$$

Here, f is the attachment frequency of hydrate building units to the hydrate nucleus (~0.5 GHz), C_0 is the concentration of nucleation sites, and $z \approx 0.01 - 1$ is the Zeldovich factor.[14] The latter quantifies the reciprocal of the width of the nucleus region (i.e., the range of cluster sizes for which the formation energy equals that of the critical nucleus within the thermal energy $k_B T$).

The thermodynamic parameter, B', is a measure of the work required to form a critical nucleus and is given by the expression

$$B' = \frac{4c^3 v_h^2 \sigma_{ef}^3}{27 k_B\, \Delta s_e^2} \tag{3}$$

Here, c is a shape factor ($=(36\pi)^{1/3}$ for spherical, cap, or lens-shaped clusters); k_B is the Boltzmann constant; v_h is the volume of a hydrate building unit containing one gas molecule and n_w water molecules, where for sI CH_4 hydrates, $v_h = 0.216\ nm^3$ ($n_w = 5.75$), whereas for the sII hydrates formed from the gas mixture, $v_h = 0.647\ nm^3$ ($n_w = 5.67$); $\Delta s_e = 21.1 k_B$ for CH_4 hydrates and $17.9 k_B$ for the gas mixture;[16] and $\sigma_{ef} = \Psi\sigma$ is the effective surface free energy of the hydrate−solution interface. Kashchiev and Firoozabadi took $\sigma = 20\ mJ\cdot m^{-2}$ on the basis of estimates of the surface free energy of water−ice interfaces.[14] The quantity Ψ is a number between 0 and 1 that can be calculated from the substrate/hydrate/fluid contact angle, θ, via

$$\psi = \left[\frac{1}{4}(2 + \cos\theta)(1 - \cos\theta)^2\right]^{1/3} \tag{4}$$

The contact angle is set via Young's equation by the differences in the surface free energies of the three interfaces. If the contact angle is 180° (i.e., completely nonwetting), $\Psi = 1$ and σ_{ef} is equivalent to the surface free energy of the water−hydrate interface, as would be applicable to homogeneous nucleation of a spherical cluster. For heterogeneous nucleation, the size and shape of the cluster is affected by the hydrate−substrate interaction, resulting in $\Psi < 1$.

For systems in which the time required to detect a new phase is limited only by the nucleation rate, (i.e., subject to the mononuclear nucleation mechanism), the probability of observing hydrate formation as a function of time for a constant driving force is given by[13]

$$P(t) = 1 - \exp(-J^* t) \tag{5}$$

where J^* is the stationary nucleation rate given by eq 1 multiplied by either the sample volume V for homogeneous nucleation in the bulk or the interfacial area a for heterogeneous nucleation. Under the assumption that the time lag required to reach the stationary nucleation rate at a given subcooling is negligible compared with the time taken to change the subcooling (i.e., the experimental cooling rate is comparatively slow), eq 1 can be substituted into eq 5 to provide a functional form to represent the measured cumulative subcooling formation probability distributions. Replacing t in eq 1 by $\Delta T/\beta$, where β is the cooling ramp rate gives

$$P(\Delta T) = 1 - \exp\left(-aA\, \exp\left(\frac{\Delta s_e\, \Delta T}{k_B T}\right) \exp\left(-\frac{B'}{T\Delta T^2}\right)\Delta T/\beta\right) \tag{6}$$

for heterogeneous nucleation. If an independent estimate of a is available, regression of the measured subcooling formation probability distributions to this working equation by treating B' and A as adjustable parameters allows direct comparisons of experiment with the predictions of nucleation theory. In the least squares objective function constructed using eq 6, the adjustable parameters B' and A are somewhat orthogonal, with B' principally determining the location of the distribution's median subcooling and A principally determining the distribution's width.

Tests of Theory and Kinetic Inhibitor Performance. The 542 point subcooling formation probability distribution measured for pure CH_4 at 700 rpm was regressed to eq 6, as were subcooling formation probability distributions measured at 700 rpm for the sII-forming natural gas mixture, with varying concentrations of the commercial KHI, Luvicap EG (BASF Global Oilfield Solutions). In the Luvicap EG formulation, the polymer polyvinylcapralactam is delivered in an ethylene glycol solvent at a concentration of 41 wt %. Although ethylene glycol is a thermodynamic hydrate inhibitor,[33] when the KHI concentration is ≤1 wt % of the aqueous phase, the ethylene glycol has a negligible effect on the hydrate equilibrium temperature, shifting it by only 0.2 K. Figure 5 shows the formation probability distributions, each with more than 100 data points, measured for the gas mixture in the presence of 0, 0.5, and 1 wt % KHI. Results from the least square regressions of eq 6 to the data are listed in Table 1.

The formation probability distributions measured at 700 rpm for pure CH_4 and the gas mixture in the absence of KHI are quite

DOI: 10.1021/acs.langmuir.7b03901
Langmuir XXXX, XXX, XXX−XXX

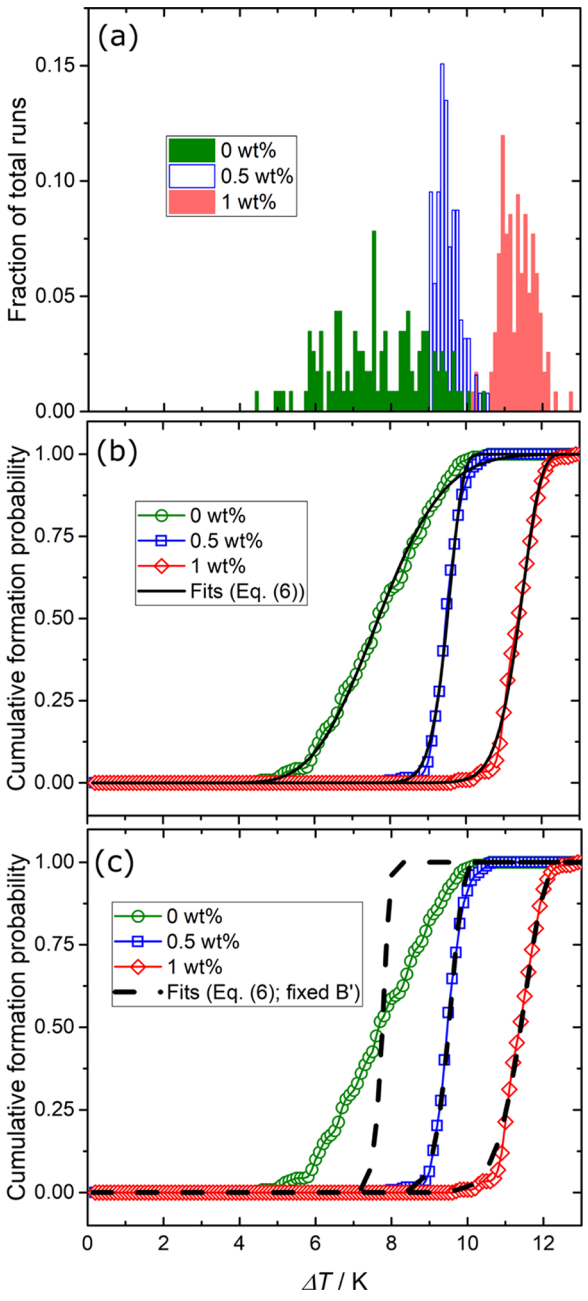

Figure 5. Hydrate formation probability distributions for the gas mixture with varying concentrations of the kinetic hydrate inhibitor (KHI), Luvicap EG, in the aqueous phase. (a) Probability density of hydrate formation and (b, c) calculated cumulative formation probability versus subcooling, ΔT. The shear rate and regeneration temperature were, respectively, 700 rpm and 20 °C. The initial condition was 8.5 MPa at 20 °C. The solid black lines in (b) are fits of eq 6 to each data set. The dashed black lines in (c) are fits of eq 6 to each data set while keeping B' fixed at 4.4×10^5 K^3. The best-fit parameter values are listed in Table 1: these compare reasonably with theoretical expectations of B' based on eq 3 but are quite different from theoretical expectations of A based on eq 2.

similar, with average subcoolings of 6.45 ± 0.07 and 7.65 ± 0.12 K, respectively, and standard deviations of 1.6 and 1.3 K, respectively. The addition of the KHI had two primary effects relative to the baseline formation distribution obtained for the gas mixture in the absence of Luvicap EG: it (i) increased the average subcooling (by almost 4 K at 1 wt %) and (ii) decreased the standard deviation of the hydrate formation probability distribution (by a factor of around 3). Consequently, the KHI can be seen to suppress hydrate formation both by translating the probability distribution to higher subcoolings and by making it more deterministic and less stochastic.

These qualitative differences in the distributions are reflected in the numerical best-fit values of A and B' when they were both treated as adjustable parameters in the regression of eq 6 to the measured cumulative formation probability distributions. These fits, shown as black solid lines in Figure 5b, reproduced the measured distributions well, with a root mean square deviation of 0.02 or less in all cases. To obtain the fits, we employed the NonlinearModelFit function in Mathematica 10.1 (Wolfram Research Inc.), which used the Levenberg−Marquardt algorithm and was relatively robust with respect to the choice of the initial values of A and B'. On the basis of the nucleation model of Kashchiev and Firoozabadi[14] discussed above, the surface area available for nucleation was assumed to be only the water−stainless steel interface and hence a was set equal to 6 cm^2 in eq 6.

Nucleation theory can be used to try and interpret the best-fit values of B' and A obtained for the regression using eqs 2−4. This comparison with theory works best for the thermodynamic parameter. The best-fit values of B' obtained for pure CH_4 and the gas mixture in the absence of KHI (Table 1) correspond to contact angles for the hydrate nucleus on the steel−water interface of 22 and 14°, respectively. The factor of 10 increase in the best-fit values of B' for the gas mixture obtained in the presence of the KHI corresponds to an increase in the contact angle to 24−26°. Nevertheless, both of these suggest that hydrate preferentially "wets" steel, which is consistent with the initial assumption that this interface is energetically favorable for nucleation.

On the other hand, the best-fit values of A (Table 1) are vastly smaller than the theoretical estimates reported by Kashchiev and Firoozabadi of $A = 4 \times 10^{26}$ m^{-2}·s^{-1} for heterogeneous nucleation.[14] Such a value of A would produce subcooling formation probability distributions that approach step functions, with virtually no width measurable within the finite temperature resolution of the HPS-ALTA. The fact that much greater distribution widths are observed in these and all other reported experimental hydrate formation probability distributions suggests that some other phenomenon, likely acting on macroscopic length scales and not considered by nucleation theory, is responsible for the stochastic nature of the measurements.

Nevertheless, whatever gives rise to this macroscopic stochastic behavior is suppressed significantly in the presence of the KHI. This observation implies that the values of B' and thus θ extracted from the KHI-based data are more representative than those obtained from the inhibitor-free distributions because of correlations between the parameters adjusted during the regression; a 10-fold change in B' caused by a change in A by a factor of 10^5 may be considered a relatively weak correlation. Accordingly, we refit all of the measured high-shear distributions with B' constrained at 4.4×10^5 K^3 ($\theta = 25.2°$ for the gas mixture) and the kinetic parameter as the only adjustable variable (denoted as A^* for clarity). The results show that the averages of the observed distributions can be represented by the same thermodynamic parameter and that the apparent variation in the θ obtained with and without KHI could well be an artifact of parameter correlation. Furthermore, although not representing the distribution widths measured for systems without KHI, the values of A^* do follow a decreasing trend with increasing KHI concentration, which is consistent with the inhibition mechanism

DOI: 10.1021/acs.langmuir.7b03901
Langmuir XXXX, XXX, XXX−XXX

Table 1. Values of Best-Fit Parameters B' and A Obtained by Regression of eq 6 to the Measured Formation Probability Distributions, with Corresponding Values of Ψ and θ Derived from B'[a]

gas	KHI/wt %	B'/K^3	Ψ	θ/deg	$A/m^{-2}\cdot s^{-1}$	$A^*/m^{-2}\cdot s^{-1}$
pure CH_4	0	2.1×10^4	0.39	22	21	1×10^{15}
mixture	0	4.3×10^4	0.09	14	40	4.1×10^{11}
mixture	0.5	3.9×10^5	0.18	24	9.6×10^6	6.4×10^7
mixture	1	4.9×10^5	0.19	26	1.1×10^6	2.7×10^5

[a]The values of A^* listed were obtained by constraining B' to a value of 4.4×10^5 K^3 during the regression, which, for the gas mixture, corresponds to a hydrate−substrate contact angle of 25.2°. The value of B' used in the constrained regression is the average of the values obtained from the two-parameter fits to the gas mixture data in the presence of KHI. The fits obtained for the gas mixture are shown in Figure 5.

discussed by Kashchiev and Firoozabadi,[14] namely, the suppression of nucleation sites by adsorption thereon by inhibitor molecules.

Finally, we consider the impact of the KHI on the initial growth rate of the hydrate phase. Unlike many current techniques used to qualify KHI performance, the HPS-ALTA can be used to quantify an inhibitor's suppression of formation probability separately from its suppression of subsequent growth. Figure 6a shows the pressure and temperature−time series data acquired for two individual formation measurements from systems with either deionized water or a 1 wt % KHI solution. All other experimental parameters were the same for the two measurements. The comparison of these two runs shows how the KHI not only retards hydrate formation, forcing it to occur at larger subcoolings, but also inhibits the subsequent hydrate growth. This can be seen most clearly from the difference in the final pressure values measured at the end of the cooling cycle: the pressure remains higher in the system with the KHI due to a reduced gas consumption by the hydrate phase. Figure 6c shows the initial growth-rate probability distributions for varying concentrations of KHI in the aqueous phase. As with the formation probability distributions, the addition of KHI both shifts and narrows the growth-rate distribution: growth is impeded and the growth rate is less stochastic. Interestingly, little difference was observed in the initial growth rates for 0.5 and 1 wt % KHI despite the appreciable further increase in average formation subcooling observed for the 1 wt % KHI solution.

The data shown in Figures 5 and 6 clearly illustrate the key advantages of the HPS-ALTA in the context of quantitatively assessing the performance of KHIs relative to more conventional methods, such as rocking cells and standard autoclaves. First, the resolution with which the shift in mean subcooling caused by a KHI can be determined from a conventional data set consisting of around 10 or so formation events is significantly lower than that afforded by the 100 or more measurements acquired with the HPS-ALTA in a comparable time frame. Second, without this statistically significant number of measurements, a key mechanism by which the KHI reduces the likelihood (and hence risk) of hydrate formation would remain unresolved: the 3-fold reduction in the standard deviation of the distribution. Finally, data such as those shown in Figure 6 provide the opportunity to quantify the extent to which the KHI inhibits growth in addition to delaying formation. This last capability is unique to the HPS-ALTA described here, as previous ALTA-type experiments have generally relied on visual detection of hydrate formation, with no ability to quantify the minimum amount of detectable hydrate or the rate of hydrate growth.

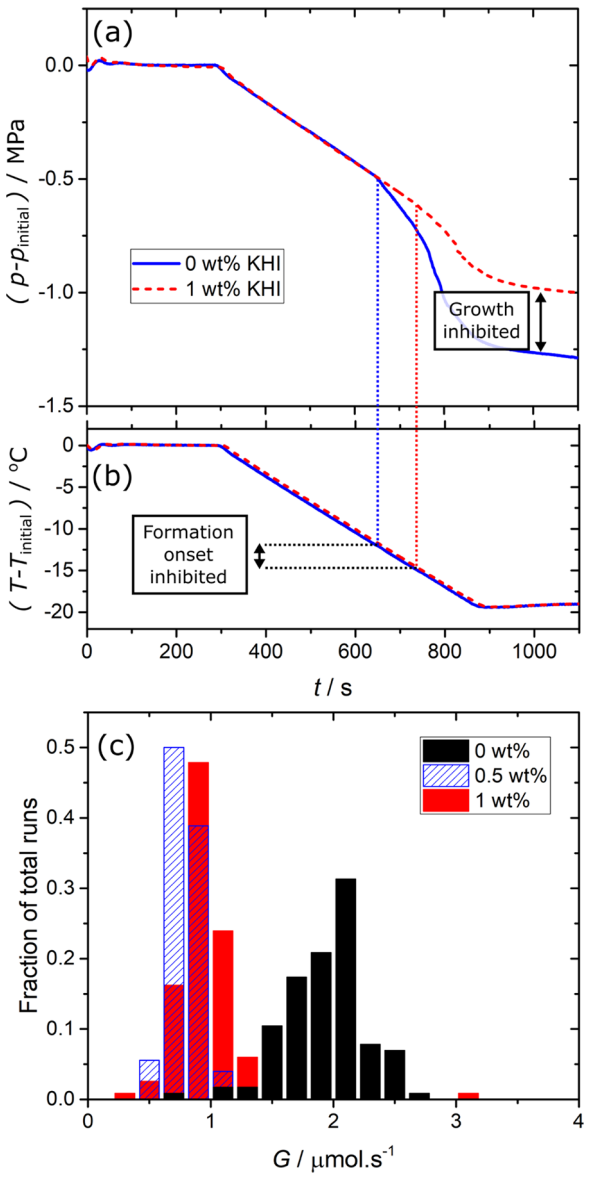

Figure 6. Example pressure (a) and temperature (b) time series data for the gas mixture obtained in two cooling ramps, one with and one without KHI present in the aqueous phase. The experimental conditions were as follows: 2 $K\cdot min^{-1}$ cooling rate, 700 rpm shear rate, regeneration temperature of 20 °C, and a 5 min holding time at the regeneration temperature. (c) Histograms for the initial growth rate, G, for the gas mixture, as quantified by the rate of gas consumption, for varying concentrations of Luvicap EG, in the aqueous phase.

DOI: 10.1021/acs.langmuir.7b03901
Langmuir XXXX, XXX, XXX−XXX

SUMMARY AND CONCLUSIONS

A new apparatus and method for experimental studies of gas hydrate formation and growth allows statistically large numbers of hydrate formation events to be measured automatically in reasonably short time frames. The use of gas consumption to infer hydrate formation means the minimum amount of hydrate formation detectable can be quantitatively estimated at around 1 μmol (or 17 μg), corresponding to a maximum delay of ~3 s from the actual nucleation event to experimental detection. Critically, the application of shear during gas hydrate experiments with an ALTA was demonstrated for the first time, allowing the impact of mass-transfer limitations on the measured formation distributions to be assessed. For the cell geometry used in this work, a shear rate of 700 rpm was shown to effectively eliminate mass-transfer limitations, as demonstrated by the consistency of measured growth rates with values predicted using the method of Turner et al.[5]

The KHI data acquired provided measures of the chemical's effect on (i) increase in mean subcooling, (ii) reducing the distribution's width, and (iii) suppressing the initial growth rate. Although one or all three of these factors may be central to the selection of a KHI for operational purposes, conventional performance tests with autoclaves or rocking typically provide insight into only one of these attributes or, at best, an amalgam of average delay and growth-rate suppression. Additional information about how a particular KHI achieves a given level of performance may facilitate improvements.

Comparisons with the predictions of the nucleation theory framework presented by Kashchiev and Firoozabadi[14] for gas hydrates were made with formation probability distributions measured at the maximum achievable shear rate. Experimental values for the thermodynamic parameter B' were consistent with theoretical predictions, given steel−hydrate−water contact angles of 14−26°. In contrast, however, the experimental values of the kinetic parameter A differ significantly from those predicted by theory. This suggests that the observed distribution widths, which are much larger than would be expected on the basis of considerations of microscopic processes, are the result of phenomena acting over macroscopic length scales. Addition of a KHI caused the value of A extracted from the measured distributions to increase toward the theoretical value; potentially such inhibitors could be used to suppress the macroscopic effects that broaden distributions and facilitate further tests of theory.

AUTHOR INFORMATION

Corresponding Author

*E-mail: eric.may@uwa.edu.au.

ORCID

Eric F. May: 0000-0001-5472-6921

Zachary M. Aman: 0000-0003-4496-3303

Notes

The authors declare no competing financial interest.

ACKNOWLEDGMENTS

This work was funded by Shell and the Australian Research Council through DP150100341 and also IC15001019 as part of the ARC Training Centre for LNG Futures. The HPS-ALTA was initially designed and constructed by Reuben Wu and David Amm. P.L.S. was the recipient of an Australian Research Council Discovery Early Career Award (project number DE140101094) funded by the Australian Government. We thank Sebastian Schulze, Aslan Goskan, and Juwoon Park for their contributions to the experiments and data analysis routines.

REFERENCES

(1) Sloan, E. D. A changing hydrate paradigm-from apprehension to avoidance to risk management. *Fluid Phase Equilib.* **2005**, *228−229*, 67−74.

(2) Makogon, Y. F. *Hydrates of Hydrocarbons*; PennWell Publishing Company: Tulsa, OK, 1997; p 482.

(3) Maeda, N.; Wells, D.; Hartley, P. G.; Kozielski, K. A. Statistical Analysis of Supercooling in Fuel Gas Hydrate Systems. *Energy Fuels* **2012**, *26*, 1820−1827.

(4) Abay, H. K.; Svartaas, T. M. Effect of Ultralow Concentration of Methanol on Methane Hydrate Formation. *Energy Fuels* **2010**, *24*, 752−757.

(5) Turner, D.; Boxall, J.; Yang, S.; Kleehamer, D.; Koh, C.; Miller, K.; Sloan, E. D.; Xu, Z.; Mathews, P.; Talley, L. In *Development of a Hydrate Kinetic Model and its Incorporation into the OLGA2000 Transient Multi-Phase Flow Simulator*, Fifth International Conference on Gas Hydrates, Trondheim, Norway, 2005.

(6) Matthews, P. N.; Notz, P. K.; Widener, M. W.; Prukop, G. Flow Loop Experiments Determine Hydrate Plugging Tendencies in the Field. *Ann. N. Y. Acad. Sci.* **2000**, *912*, 330−338.

(7) Askvik, K. M. In *Natural Kinetic Inhibition of Gas Hydrates in Oil and Gas Production*, 9th International Conference on Gas Hydrates, Denver, CO, 2017.

(8) Glenat, P.; Devoisselle, R.; Pegazy, L.; Bourg, P.; Pere, M.; Arnault, R. In *Natural Kinetic Hydrates Inhibitors of Crude Oils*, 9th International Conference on Gas Hydrates, Denver, CO, 2017.

(9) Nagappayya, S. G.; Bartels, J. W. In *Old Technology, New Market - Low Dosage Hydrate Inhibitor in US Onshore*, 9th International Conference on Gas Hydrates, Denver, CO, 2017.

(10) Sinquin, A.; Oral, O.; Rivereau, A.; Glenta, P.; Devoisselle, R. In *Commercial Anti-Agglomerates Ways of Action in Simple Gas/Condensate/Water Systems*, 9th International Conference on Gas Hydrates, Denver, CO, 2017.

(11) May, E. F.; Marsh, K. N.; Goodwin, A. R. H. Frontier Oil and Gas: Deep-Water and the Arctic. In *Future Energy: Improved, Sustainable and Clean Options for our Planet*, 2nd ed.; Letcher, T., Ed.; Elsevier, 2014; pp 75−93.

(12) Ke, W.; Kelland, M. A. Kinetic Hydrate Inhibitor Studies for Gas Hydrate Systems: A Review of Experimental Equipment and Test Methods. *Energy Fuels* **2016**, *30*, 10015−10028.

(13) Kashchiev, D. *Nucleation: Basic Theory with Applications*; Butterworth-Heinemann: U.K., 2000.

(14) Kashchiev, D.; Firoozabadi, A. Nucleation of gas hydrates. *J. Cryst. Growth* **2002**, *243*, 476−489.

(15) Kashchiev, D.; Firoozabadi, A. Induction time in crystallization of gas hydrates. *J. Cryst. Growth* **2003**, *250*, 499−515.

(16) Kashchiev, D.; Firoozabadi, A. Driving force for crystallization of gas hydrates. *J. Cryst. Growth* **2002**, *241*, 220−230.

(17) Svartaas, T. M.; Ke, W.; Tantciura, S.; Bratland, A. U. Maximum Likelihood Estimation-A Reliable Statistical Method for Hydrate Nucleation Data Analysis. *Energy Fuels* **2015**, *29*, 8195−8207.

(18) Ke, W.; Svartaas, T. M.; Abay, H. K. In *An Experimental Study on SI Hydrate Formation in Presence of Methanol, PVP and PVCAP in an Isochoric Cell*, 7th International Conference on Gas Hydrates (ICGH 2011), Edinburgh, Scotland, United Kingdom, 2011.

(19) Ke, W.; Svartaas, T. M. In *Effects of Stirring and Cooling on Methane Hydrate Formation in a High-Pressure Isochoric Cell*, 7th International Conference on Gas Hydrates (ICGH 2011), Edinburgh, Scotland, United Kingdom, 2011.

(20) Lone, A.; Kelland, M. A. Exploring Kinetic Hydrate Inhibitor Test Methods and Conditions Using a Multicell Steel Rocker Rig. *Energy Fuels* **2013**, *27*, 2536−2547.

(21) Wilson, P. W.; Lester, D.; Haymet, A. D. J. Heterogeneous nucleation of clathrates from supercooled tetrahydrofuran (THF)/water mixtures, and the effect of an added catalyst. *Chem. Eng. Sci.* **2005**, *60*, 2937−2941.

DOI: 10.1021/acs.langmuir.7b03901
Langmuir XXXX, XXX, XXX−XXX

(22) Barlow, T. W.; Haymet, A. D. J. ALTA - an Automated Lag-Time Apparatus for Studying the Nucleation of Supercooled Liquids. *Rev. Sci. Instrum.* **1995**, *66*, 2996−3007.
(23) Maeda, N. Measurements of gas hydrate formation probability distributions on a quasi-free water droplet. *Rev. Sci. Instrum.* **2014**, *85*, No. 065115.
(24) Sowa, B.; Maeda, N. Statistical Study of the Memory Effect in Model Natural Gas Hydrate Systems. *J. Phys. Chem. A* **2015**, *119*, 10784−10790.
(25) May, E. F.; Wu, R.; Kelland, M. A.; Aman, Z. M.; Kozielski, K. A.; Hartley, P. G.; Maeda, N. Quantitative kinetic inhibitor comparisons and memory effect measurements from hydrate formation probability distributions. *Chem. Eng. Sci.* **2014**, *107*, 1−12.
(26) Maeda, N. Development of a high pressure electrical conductivity probe for experimental studies of gas hydrates in electrolytes. *Rev. Sci. Instrum.* **2013**, *84*, No. 015110.
(27) Sowa, B.; Zhang, X. H.; Kozielski, K. A.; Dunstan, D. E.; Hartley, P. G.; Maeda, N. Study of electrical conductivity response upon formation of ice and gas hydrates from salt solutions by a second generation high pressure electrical conductivity probe. *Rev. Sci. Instrum.* **2014**, *85*, No. 115101.
(28) Elliott, C.; Vijayakumar, V.; Zink, W.; Hansen, R. National Instruments LabVIEW: A Programming Environment for Laboratory Automation and Measurement. *JALA* **2007**, *12*, 17−24.
(29) McKinney, W. In *Data Structures for Statistical Computing in Python*, Proceedings of the 9th Python in Science Conference, Austin, TX; van der Walt, S., Millman, J., Eds.; Austin, TX, 2010; pp 51−56.
(30) Hunter, J. D. Matplotlib: A 2D graphics environment. *Comput. Sci. Eng.* **2007**, *9*, 90−95.
(31) van der Walt, S.; Colbert, S. C.; Varoquaux, G. The NumPy Array: A Structure for Efficient Numerical Computation. *Comput. Sci. Eng.* **2011**, *13*, 22−30.
(32) Akhfash, M.; Arjmandi, M.; Aman, Z. M.; Boxall, J.; May, E. F. Gas Hydrate Thermodynamic Inhibition with MDEA for Reduced MEG Circulation. *J. Chem. Eng. Data* **2017**, *62*, 2578−2583.
(33) Sloan, E. D.; Koh, C. A. *Clathrate Hydrates of Natural Gases*, 3rd ed.; CRC Press: Boca Raton, FL, 2007.
(34) Vysniauskas, A.; Bishnoi, P. R. A Kinetic-Study of Methane Hydrate Formation. *Chem. Eng. Sci.* **1983**, *38*, 1061−1072.
(35) Englezos, P.; Kalogerakis, N.; Dholabhai, P. D.; Bishnoi, P. R. Kinetics of Gas Hydrate Formation from Mixtures of Methane and Ethane. *Chem. Eng. Sci.* **1987**, *42*, 2659−2666.

DOI: 10.1021/acs.langmuir.7b03901
Langmuir XXXX, XXX, XXX−XXX